Published for SISSA by Springer

Received: *March 28, 2025*
Revised: *May 31, 2025*
Accepted: *July 14, 2025*
Published: *August 8, 2025*

First observation of $\Lambda_c(2595)^+ \to \Lambda_c^+\pi^0\pi^0$ and $\Lambda_c(2625)^+ \to \Lambda_c^+\pi^0\pi^0$

The BESIII collaboration

E-mail: besiii-publications@ihep.ac.cn

Abstract: By analysing e^+e^- annihilation data corresponding to an integrated luminosity of 368.48 pb^{-1} collected at the centre-of-mass energies of $\sqrt{s} = 4.918$ and 4.951 GeV with the BESIII detector, we report the first observation of $\Lambda_c(2595)^+$ and $\Lambda_c(2625)^+ \to \Lambda_c^+\pi^0\pi^0$ with statistical significances of 7.9σ and 11.8σ, respectively. The branching fractions of $\Lambda_c(2595)^+$ and $\Lambda_c(2625)^+ \to \Lambda_c^+\pi^0\pi^0$ are measured to be $(59.5 \pm 11.1_{\text{stat.}} \pm 7.9_{\text{syst.}})\%$ and $(41.0 \pm 5.2_{\text{stat.}} \pm 3.3_{\text{syst.}})\%$, respectively. The absolute branching fraction of $\Lambda_c(2595)^+$ is consistent with the expectation of the mechanism referred to as the *threshold effect*, proposed for the strong decays of $\Lambda_c(2595)^+$ within uncertainty.

Keywords: Branching fraction, Charm Physics, e^+-e^- Experiments

ArXiv ePrint: 2503.21413

https://doi.org/10.1007/JHEP08(2025)065

JHEP08(2025)065

Contents

1 Introduction

Charmed baryon spectroscopy provides an ideal platform for studying the dynamics of light quarks in the presence of a heavy quark. The strong decays of charmed baryons are most conveniently described by heavy hadron chiral perturbation theory, in which heavy quark symmetry and chiral symmetry are incorporated [1, 2]. The chiral Lagrangian involves several coupling constants for transitions between s-wave and p-wave charmed baryons, referred to as $h_2 - h_{15}$ defined in ref. [3, 4]. Among these, the coupling constants h_2 and h_8 can be extracted from the strong decays of $\Lambda_c(2595)^+$ and $\Lambda_c(2625)^+$ [5, 6]. These couplings are critical to describe the charmed baryon spectrum and to make predictions of decays into other charmed baryons. However, to date, the strong decays of $\Lambda_c(2595)^+$ and $\Lambda_c(2625)^+$ remain poorly understood due to the lack of experimental data [7]. The existing determinations of h_2 and h_8 are based on the measured decay widths of $\Lambda_c(2595)^+$ and $\Lambda_c(2625)^+$. Since the width of $\Lambda_c(2625)^+$ is nearly zero [7, 8], only the upper limit on h_8 is provided. A precise measurement of the strong decays of $\Lambda_c(2595)^+$ and $\Lambda_c(2625)^+$ is highly desirable. The corresponding branching fractions (BFs) are important inputs for determining h_2 and h_8.

In the quark model, the $\Lambda_c(2595)^+$ and $\Lambda_c(2625)^+$ are the lowest-lying excited states of Λ_c^+ with spin-parities of $1/2^-$ and $3/2^-$, respectively, and form a degenerate pair of the p-wave state [5, 6]. The upper limit on the absolute BF of the decay $\Lambda_c(2595)^+ \to \Lambda_c^+\pi^+\pi^-$ was determined to be less than 85.0% [9] at the 90% confidence level. The absolute BF of the process $\Lambda_c(2625)^+ \to \Lambda_c^+\pi^+\pi^-$ has been measured to be $(51.1 \pm 5.8_{\rm stat.} \pm 3.5_{\rm syst.})\%$ [9]. However, the absolute BFs of these $\pi^0\pi^0$ transitions have, until now, never been measured experimentally. Given that only an upper limit on the absolute BF has been obtained for the decay $\Lambda_c(2595)^+ \to \Lambda_c^+\pi^+\pi^-$, measuring the absolute BF of the decay $\Lambda_c(2595)^+ \to \Lambda_c^+\pi^0\pi^0$ becomes increasingly important. Assuming isospin symmetry, the ratio between the BFs

JHEP08(2025)065

of $\pi^+\pi^-$ and $\pi^0\pi^0$ transitions is 2:1, which forms the basis for the BFs of various strong $\Lambda_c(2595)^+$ and $\Lambda_c(2625)^+$ decays quoted in the Particle Data Group (PDG) [7]. However, isospin symmetry in these processes has not been verified by any experimental measurement. In ref. [10], a mechanism known as the *threshold effect* is proposed to account for the limited transition phase space in these strong decays. If this mechanism applies here as well, it would break the 2:1 relation between $\pi^+\pi^-$ and $\pi^0\pi^0$ transitions in $\Lambda_c(2595)^+$ decay.

In this paper, we report the first measurement of the absolute BFs of $\Lambda_c(2595)^+$ and $\Lambda_c(2625)^+ \to \Lambda_c^+\pi^0\pi^0$, obtained from the processes of $e^+e^- \to \bar{\Lambda}_c^-\Lambda_c(2595)^+ + c.c.$ and $\bar{\Lambda}_c^-\Lambda_c(2625)^+ + c.c.$. We use the data collected with the BESIII detector at centre-of-mass (c.m.) energies $\sqrt{s} = 4.918$ and 4.951 GeV [11]. The integrated luminosities of the data samples at 4.918 and 4.951 GeV are 208.1 and 160.4 pb^{-1} [12], respectively.

2 BESIII detector and Monte Carlo simulation

The BESIII detector [13] records symmetric e^+e^- collisions provided by the BEPCII [14] storage ring, which operates in the center-of-mass energy ($\sqrt{s}$) range from 1.84 to 4.95 GeV, with a peak luminosity of 1×10^{33} cm^{-2}s^{-1} achieved at $\sqrt{s} = 3.77$ GeV. BESIII has collected large data samples at these energy regions [15]. The cylindrical core of the BESIII detector covers 93% of the full solid angle and consists of a helium-based multilayer drift chamber (MDC), a plastic scintillator time-of-flight system (TOF), and a CsI(Tl) electromagnetic calorimeter (EMC), which are all enclosed in a superconducting solenoidal magnet providing a 1.0 T magnetic field [16]. The solenoid is supported by an octagonal flux-return yoke with resistive plate counter based muon identification modules interleaved with steel. The charged-particle momentum resolution at 1 GeV/c is 0.5%, and resolution of the ionization energy loss in the MDC (dE/dx) is 6% for electrons from Bhabha scattering. The EMC measures photon energies with a resolution of 2.5% (5%) at 1 GeV in the barrel (end-cap) region. The time resolution in the TOF barrel region is 68 ps, while that in the end-cap region is 110 ps. The end-cap TOF system was upgraded in 2015 using multi-gap resistive plate chamber technology, providing a time resolution of 60 ps [17, 18].

Simulated samples are produced with a Geant4-based [19] Monte Carlo (MC) toolkit, which includes a full implementation of the detector geometry and response [16] of the BESIII detector. The simulations are used to determine the efficiency of the detector and the reconstruction, and to estimate the background. The inclusive MC samples, which consists of $\Lambda_c^+\bar{\Lambda}_c^-$ events, $D_{(s)}$ production, ψ states produced in initial state radiation processes, and continuum processes $e^+e^- \to q\bar{q}$ ($q = u, d, s$), is generated to estimate the potential background. Here, all the known decay modes of charmed hadrons and charmonia are modeled with EVTGEN [20, 21] using BFs taken from the PDG [7], while the remaining unknown decays are modeled with LUNDCHARM [22, 23]. Final state radiation from charged final state particles is incorporated using PHOTOS [24].

3 Measurement method

This analysis is performed to search for the signal processes $\Lambda_c(2595)^+ \to \Lambda_c^+\pi^0\pi^0$ and $\Lambda_c(2625)^+ \to \Lambda_c^+\pi^0\pi^0$, based on the productions $e^+e^- \to \bar{\Lambda}_c^-\Lambda_c(2595)^+$ and $\bar{\Lambda}_c^-\Lambda_c(2625)^+$,

JHEP08(2025)065

and to measure their BFs in a model-independent approach. Firstly, three hadronic decay modes are used to reconstruct the $\bar{\Lambda}_c^-$ candidates, which are referred to as tagged $\bar{\Lambda}_c^-$ hereafter. These three hadronic decay modes are $\bar{\Lambda}_c^- \to \bar{p}K^+\pi^-$, $\bar{p}K_S^0$, and $\bar{\Lambda}\pi^-$, where the subsequent decay modes of the intermediate states are $K_S^0 \to \pi^+\pi^-$ and $\bar{\Lambda} \to \bar{p}\pi^+$. Then, we search for the signals $\Lambda_c^{*+} \to \Lambda_c^+\pi^0\pi^0$ on the recoiling side against the $\bar{\Lambda}_c^-$. Here, Λ_c^{*+} represents either $\Lambda_c(2595)^+$ or $\Lambda_c(2625)^+$.

The BFs of $\Lambda_c^{*+} \to \Lambda_c^+\pi^0\pi^0$ are determined as,

$$\mathcal{B} = \frac{(N^{\rm obs}_{\Lambda_c^{*+}} - N_{\rm bkg}) \cdot \sum_i \mathcal{B}^i_{\rm tag}\epsilon^i_{\rm tag}}{N_{\rm tag} \cdot \sum_i \mathcal{B}^i_{\rm tag}\epsilon^i_{\rm sig}}, \tag{3.1}$$

where i represents each tag mode, $\mathcal{B}_{\rm tag}$ denotes the BFs of the tag modes, $\epsilon_{\rm tag}$ corresponds to the efficiencies of reconstructing the tagged $\bar{\Lambda}_c^-$, and $\epsilon_{\rm sig}$ represents the efficiencies of selecting the signals $\Lambda_c^{*+} \to \Lambda_c^+\pi^0\pi^0$ together with the tagged $\bar{\Lambda}_c^-$, as listed in table 1 and table 2. The $N_{\rm tag}$ stands for the number of total events for $\Lambda_c(2595)^+$ or $\Lambda_c(2625)^+$ after selecting the tagged $\bar{\Lambda}_c^-$. The $N^{\rm obs}_{\Lambda_c^{*+}}$ is the number of observed events for signal $\Lambda_c^{*+} \to \Lambda_c^+\pi^0\pi^0$. Due to the fact that the energy of the photons is always lower than 150 MeV, the efficiency of detecting all four γ's from the two π^0's is only 10%. Therefore, we have adopted a partial reconstruction strategy to increase the efficiency of selecting the signal $\Lambda_c^{*+} \to \Lambda_c^+\pi^0\pi^0$, rather than full reconstruction. The peaking background contamination originated from the sources $\Lambda_c^{*+} \to \Lambda_c^+\pi^+\pi^-$ will be subtracted, and the corresponding number of events is denoted as $N_{\rm bkg}$.

The signal MC samples of $e^+e^- \to \bar{\Lambda}_c^-\Lambda_c(2595)^+/\bar{\Lambda}_c^-\Lambda_c(2625)^+ \to \bar{\Lambda}_c^-\Lambda_c^+\pi^0\pi^0$ are generated for the individual c.m. energies using the generator KKMC [25], incorporating initial state radiation effects and beam energy spread. To achieve a more accurate simulation, the polar angle (θ) distributions of $\Lambda_c(2595)^+$ and $\Lambda_c(2625)^+$ are considered in the generator via a parametrization of $f(\cos\theta) \propto (1 + \alpha_{\Lambda_c}\cos^2\theta)$. For $e^+e^- \to \bar{\Lambda}_c^-\Lambda_c(2625)^+$, the α_{Λ_c} is assigned to the measured values in ref. [26], while for $e^+e^- \to \bar{\Lambda}_c^-\Lambda_c(2595)^+$, the α_{Λ_c} is set to 1. Additionally, any possible deviations from these values are considered as a source of systematic uncertainty. The $\bar{\Lambda}_c^-$ is required to decay into the three tag modes, while the Λ_c^+ decays into any allowed final states. The input line shapes for their cross sections are also obtained from ref. [26]. The charge-conjugate processes $e^+e^- \to \Lambda_c^+\bar{\Lambda}_c(2595)^-$ and $\Lambda_c^+\bar{\Lambda}_c(2625)^-$ are similarly generated with $\bar{\Lambda}_c(2595)^-$ and $\bar{\Lambda}_c(2625)^- \to \bar{\Lambda}_c^-\pi^0\pi^0$, where the Λ_c^+ subsequently decays to any allowed processes and the $\bar{\Lambda}_c^-$ decays to the three tag modes. These signal MC samples are used to extract the signal shapes and efficiencies $\epsilon^i_{\rm sig}$.

Moreover, to extract the total yields $N_{\rm tag}$ and corresponding efficiencies $\epsilon^i_{\rm tag}$, additional MC samples of $e^+e^- \to \bar{\Lambda}_c^-\Lambda_c(2595)^+$ and $\bar{\Lambda}_c^-\Lambda_c(2625)^+$ are generated with the $\bar{\Lambda}_c^-$ decaying into the three tag modes and the Λ_c^{*+} into any allowed processes. Their charge-conjugate processes $e^+e^- \to \Lambda_c^+\bar{\Lambda}_c(2595)^-$ and $\Lambda_c^+\bar{\Lambda}_c(2625)^-$ are produced with the Λ_c^+ decaying into any allowed processes and the $\bar{\Lambda}_c^-$ into the three tag modes. The decays of $\Lambda_c(2595)^+$ and $\Lambda_c(2625)^+$ are modelled based on the information in the PDG [7], with both decaying into $\Lambda_c^+\pi^+\pi^-$ and $\Lambda_c^+\pi^0\pi^0$ final states.

In the analysis, the events with $\bar{\Lambda}_c^- \to \bar{p}K^+\pi^-$, $\bar{p}K_S^0$, and $\bar{\Lambda}\pi^-$ are selected in the meantime, which correspond to the charge-conjugate modes of tagged $\bar{\Lambda}_c^-$ and are referred to

JHEP08(2025)065

as tagged Λ_c^+. Signal MC samples are also generated for the tagged Λ_c^+, which are exactly the same as those for tagged $\bar{\Lambda}_c^-$. For simplicity, throughout this paper, only cases with tagged $\bar{\Lambda}_c^-$ are described, while those with charge-conjugate mode of tagged Λ_c^+ are implicitly included.

4 Selection for tagged $\bar{\Lambda}_c^-$ and extraction of the number of total events for Λ_c^{*+}

Charged tracks detected in the helium-based MDC are required to be within a polar angle (θ) range of $|\cos\theta| < 0.93$, where θ is defined with respect to the z-axis. The distance of closest approach for charged tracks that do not come from a Λ or K_S^0 decay are required to be within ± 10 cm along the z-axis and 1 cm in the plane perpendicular to the beam. The particle identification (PID) is implemented by combining measurements of the specific ionization energy loss in the MDC and the TOF between the interaction point and the dedicated TOF detector system. Each charged track that doesn't come from K_S^0 and $\bar{\Lambda}$ is assigned a particle type of pion, kaon or proton, according to which assignment has the highest probability. For the mode $\bar{\Lambda}_c^- \to \bar{p}K^+\pi^-$, a vertex fit is performed to each $\bar{p}K^+\pi^-$ combination candidate, and the re-fitted momenta are used in the further study.

Candidates for K_S^0 and $\bar{\Lambda}$ are reconstructed by their dominant modes $K_S^0 \to \pi^+\pi^-$ and $\bar{\Lambda} \to \bar{p}\pi^+$, respectively, where the charged tracks are required to have distances of closest approaches to the interaction point that are within ± 20 cm along the z-axis. To improve the signal purity, the PID requirement is only applied to the (anti)proton candidate, but not for the charged pion. A secondary vertex fit constrained by the decay vertex and the production vertex is performed to each K_S^0 or $\bar{\Lambda}$ candidate, and the re-fitted momenta are used in the further analysis. The K_S^0 or $\bar{\Lambda}$ candidate is accepted by requiring the χ^2 of the secondary vertex fit to be less than 100. Furthermore, the decay vertex is required to be separated from the interaction point by a distance of at least twice the fitted vertex resolution, and the invariant mass to be within (0.487, 0.511) GeV/c^2 for $\pi^+\pi^-$ and (1.111, 1.121) GeV/c^2 for $\bar{p}\pi^+$.

All combinations for each tag mode of $\bar{\Lambda}_c^-$ are retained, and their invariant mass, $M(\bar{\Lambda}_c^-)$, is required to fall within the range (2.27, 2.30) GeV/c^2. The recoiling mass of the tagged $\bar{\Lambda}_c^-$, $M_{\rm recoil}^{\rm tag}(\bar{\Lambda}_c^-)$, is depicted in Figure 1(a) and 1(b) by combining the three tag modes. The resonances $\Lambda_c(2595)^+$ and $\Lambda_c(2625)^+$ are observed at both energy points, indicating the existence of processes $e^+e^- \to \bar{\Lambda}_c^-\Lambda_c(2595)^+$ and $\bar{\Lambda}_c^-\Lambda_c(2625)^+$. Meanwhile, the charge-conjugate processes $e^+e^- \to \Lambda_c^+\bar{\Lambda}_c(2595)^-$ and $\Lambda_c^+\bar{\Lambda}_c(2625)^-$ distribute broadly beneath the resonances, as the tagged $\bar{\Lambda}_c^-$ can originate from the decays of $\bar{\Lambda}_c(2595)^-$ or $\bar{\Lambda}_c(2625)^-$. These productions, where the tagged $\bar{\Lambda}_c^-$ arises directly from e^+e^- collision, are denoted as $S_{ee}^{\rm tag}$, while those tagged $\bar{\Lambda}_c^-$ originates from the decays of $\bar{\Lambda}_c^{*-}$ are denoted as $S_{\rm inte}^{\rm tag}$.

An unbinned maximum likelihood fit is performed to the distribution of $M_{\rm recoil}^{\rm tag}(\bar{\Lambda}_c^-)$ (denoted as fit$_{\rm tag}$ hereafter). Both processes $S_{ee}^{\rm tag}$ and $S_{\rm inte}^{\rm tag}$ are included, and they are modelled by MC simulations in the fit$_{\rm tag}$. The two contributions are correlated with the same production cross section and individual detection efficiencies $\epsilon_{\rm tag}$. The contributions $S_{ee}^{\rm tag}$ are further convolved with Gaussian functions, which are shared between the two resonances due to the limited sample sizes at individual energy values, and account for the resolution difference between data and MC simulation. The backgrounds include contributions from continuum hadron production (denoted as $q\bar{q}$), $e^+e^- \to \Lambda_c^+\bar{\Lambda}_c^-$, $e^+e^- \to \Sigma_c\bar{\Sigma}_c$, and $e^+e^- \to \Sigma_c\bar{\Lambda}_c^-\pi$,

JHEP08(2025)065

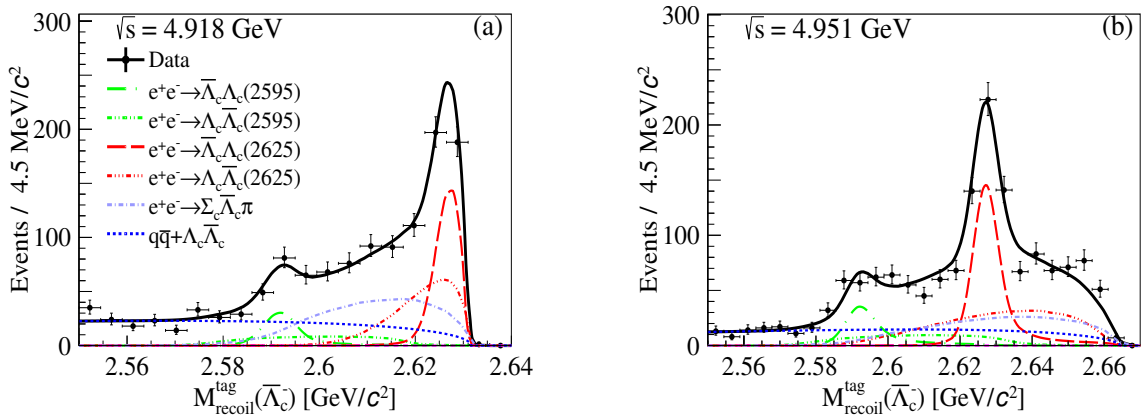

Figure 1. The fits to the distributions $M^{\rm tag}_{\rm recoil}(\bar{\Lambda}_c^-)$ at $\sqrt{s} = 4.918\,\text{GeV}$ (a) and 4.951 GeV (b). The black points with error bars are data. The solid curves represent the fit results, and the dashed curves describe individual components including both signals and backgrounds. The contribution of $e^+e^- \to \Sigma_c\bar{\Sigma}_c$ is negligible according to the fit results and cannot be seen evidently in the figures.

	$\bar{\Lambda}_c^-$ decays	$\epsilon_{\rm tag}$ (%)	$\epsilon_{\rm sig}$ (%)	$N_{\rm tag}$	$N_{\rm sig}$
$\bar{\Lambda}_c^-\Lambda_c(2595)^+$	$\bar{p}K^+\pi^-$	48.5	27.2	135.2 ± 26.4	40.3 ± 7.6
	$\bar{p}K^0_S$	49.9	26.7		
	$\bar{\Lambda}\pi^-$	38.5	20.7		
$\bar{\Lambda}_c^-\Lambda_c(2625)^+$	$\bar{p}K^+\pi^-$	46.6	27.9	418.7 ± 34.4	88.7 ± 11.3
	$\bar{p}K^0_S$	50.0	26.7		
	$\bar{\Lambda}\pi^-$	38.3	19.9		

Table 1. The detection efficiencies, $\epsilon_{\rm tag}$ and $\epsilon_{\rm sig}$, for each tag mode at $\sqrt{s} = 4.918\,\text{GeV}$. The numbers of events, $N_{\rm tag}$ and $N_{\rm sig}$ ($N^{\rm obs}_{\Lambda_c^{*+}} - N_{\rm bkg}$), combine the three tag modes.

where π denotes the isospin triplets $\pi^\pm$ and π^0, and the Σ_c denotes the triplets Σ_c^{++}, Σ_c^+, and Σ_c^0. The processes $q\bar{q}$ and $\Lambda_c^+\bar{\Lambda}_c^-$ are grouped together and modelled by ARGUS functions [27], the shape parameters of which are obtained by fitting the distributions of $M^{\rm tag}_{\rm recoil}(\bar{\Lambda}_c^-)$ in the data at $\sqrt{s} = 4.840\,\text{GeV}$ [12], which is below the Λ_c^{*+} production threshold. The magnitudes of the ARGUS functions are free parameters in the fit$_{\rm tag}$. The shapes of the contributions $e^+e^- \to \Sigma_c\bar{\Sigma}_c$ and $\Sigma_c\bar{\Lambda}_c^-\pi$ are derived from MC simulations, and their yields are determined in the fit$_{\rm tag}$. The fit results are depicted in Figure 1(a) and 1(b), where the background contributions of $e^+e^- \to \Sigma_c\bar{\Sigma}_c$ are negligible. The significances of $\Lambda_c(2595)^+$ components are 5.3σ and 8.3σ for $\sqrt{s} = 4.918$ and 4.951 GeV, respectively. The corresponding values for $\Lambda_c(2625)^+$ components are 12.7σ and 14.0σ.

5 The selection of $\Lambda_c^+\pi^0\pi^0$ candidates and extraction of the signal yields

Since the energy of the photons from the two π^0's in the signal process $\Lambda_c^{*+} \to \Lambda_c^+\pi^0\pi^0$ is less than 150 MeV, the efficiency of detecting all of them is only 10%. To improve the efficiency, a partial reconstruction strategy, relying on the topological differences, is adopted to select the signals and suppress the dominant backgrounds. Due to the presence of the

JHEP08(2025)065

	$\bar{\Lambda}_c^-$ decays	$\epsilon_{\rm tag}$ (%)	$\epsilon_{\rm sig}$ (%)	$N_{\rm tag}$	$N_{\rm sig}$
$\bar{\Lambda}_c^-\Lambda_c(2595)^+$	$\bar{p}K^+\pi^-$	48.8	22.3	210.3 ± 28.3	54.5 ± 10.2
	$\bar{p}K_S^0$	49.0	22.3		
	$\bar{\Lambda}\pi^-$	37.8	16.6		
$\bar{\Lambda}_c^-\Lambda_c(2625)^+$	$\bar{p}K^+\pi^-$	47.4	21.9	670.9 ± 55.6	114.0 ± 14.6
	$\bar{p}K_S^0$	49.6	22.4		
	$\bar{\Lambda}\pi^-$	37.6	16.6		

Table 2. The detection efficiencies, $\epsilon_{\rm tag}$ and $\epsilon_{\rm sig}$, for each tag mode at $\sqrt{s} = 4.951\,\text{GeV}$. The numbers of events, $N_{\rm tag}$ and $N_{\rm sig}$ ($N^{\rm obs}_{\Lambda_c^{*+}} - N_{\rm bkg}$), combine the three tag modes.

tagged $\bar{\Lambda}_c^-$, the dominant backgrounds to the signals originate from the processes $\Lambda_c^{*+} \to \Lambda_c^+\gamma$ and $\Lambda_c^{*+} \to \Lambda_c^+\pi^+\pi^-$. Another potential background $\Lambda_c^{*+} \to \Lambda_c^+\pi^0$ is not taken into account because it is isospin violated process and its branching fraction is highly suppressed.

To suppress the background from $\Lambda_c^{*+} \to \Lambda_c^+\gamma$ decay, we veto the events with $E_\gamma \in (0.28, 0.35)\,\text{GeV}$ for $\sqrt{s} = 4.918\,\text{GeV}$ and $E_\gamma \in (0.25, 0.38)\,\text{GeV}$ for $\sqrt{s} = 4.951\,\text{GeV}$, where E_γ represents the deposited energy of photons in the EMC. To suppress the background from $\Lambda_c^{*+} \to \Lambda_c^+\pi^+\pi^-$ decay, we require the number of charged pions with $P_{\pi^\pm} < 150\,\text{MeV}/c$ to be zero ($N_{\pi^\pm} = 0$). Here, $P_{\pi^\pm}$ represents the momentum of π^+ or π^- candidates, and the identification criteria for $\pi^\pm$ are the same as those used in the reconstruction of the tagged $\bar{\Lambda}_c^-$. Additionally, we veto events if the number of π^0 with $P_{\pi^0} < 0.15\,\text{GeV}/c$ is zero ($N_{\pi^0} > 0$), where P_{π^0} denotes the momentum of π^0. The π^0 is reconstructed with its dominant decay mode $\pi^0 \to \gamma\gamma$, and the photon candidates are identified using showers in the EMC. The deposited energy of each shower must be greater than 25 MeV in the barrel region ($|\cos\theta| \leq 0.80$) or greater than 50 MeV in the end-cap region ($0.86 \leq |\cos\theta| \leq 0.92$). To suppress electronic noise and showers unrelated to the event, the difference between the EMC time and the event start time is required to be within (0, 700) ns. The π^0 candidates are formed with a photon pair within the invariant-mass region (0.115, 0.150) GeV/c^2. To improve the resolution, a kinematic fit is performed by constraining the invariant mass of the photon pair to be the π^0 mass [7] and requiring the corresponding χ^2 of the fit to be less than 200.

With all the above selections, the signals $\Lambda_c^{*+} \to \Lambda_c^+\pi^0\pi^0$ are further investigated in the recoiling mass distribution against the tagged $\bar{\Lambda}_c^-$, $M^{\rm sig}_{\rm recoil}(\bar{\Lambda}_c^-)$, as shown in Figure 2 for both energy points. Here, the resonances $\Lambda_c(2595)^+$ and $\Lambda_c(2625)^+$ are clearly observed, indicating the signals $\Lambda_c(2595)^+$ and $\Lambda_c(2625)^+ \to \Lambda_c^+\pi^0\pi^0$. Similarly to Figure 1, the signal processes with the tagged $\bar{\Lambda}_c^-$ arising directly from e^+e^- collision are denoted as $S^{\rm sig}_{ee}$, while those with the tagged $\bar{\Lambda}_c^-$ from the decays of $\bar{\Lambda}_c^{*-}$ are denoted as $S^{\rm sig}_{\rm inte}$. Another unbinned maximum likelihood fit is performed to the distribution of $M^{\rm sig}_{\rm recoil}(\bar{\Lambda}_c^-)$ (denoted as $\text{fit}_{\rm sig}$ hereafter), where both signal contributions $S^{\rm sig}_{ee}$ and $S^{\rm sig}_{\rm inte}$ are included, and their shapes are modelled by MC simulations. The sources of non-peaking backgrounds are the same as those in the previous $\text{fit}_{\rm tag}$. The processes $q\bar{q}$ and $\Lambda_c^+\bar{\Lambda}_c^-$ are modelled using inclusive MC samples in the $\text{fit}_{\rm sig}$, with their magnitudes determined by fitting the events in the sideband region of $M(\bar{\Lambda}_c^-) \in [2.19, 2.25]\,\text{GeV}/c^2$ and $M(\bar{\Lambda}_c^-) \in [2.32, 2.38]\,\text{GeV}/c^2$. The shapes of the $e^+e^- \to \Sigma_c\bar{\Lambda}_c^-\pi$ backgrounds are modelled by MC simulations, with their magnitudes

JHEP08(2025)065

treated as free parameters in the fit_{sig}. Here, the process $e^+e^- \to \Sigma_c\bar{\Sigma}_c$ is not included, as its contribution is already negligible in the previous fit_{tag}. The resulting fitted curves are depicted in Figure 2(a) and 2(b), and the statistical significances of signals $\Lambda_c(2595)^+$ and $\Lambda_c(2625)^+ \to \Lambda_c^+\pi^0\pi^0$ are 5.3σ and 8.3σ by combining the two energy points.

Since the $\Lambda_c^{*+} \to \Lambda_c^+\pi^+\pi^-$ backgrounds exhibit similar distributions in $M^{\text{sig}}_{\text{recoil}}(\bar{\Lambda}_c^-)$ as the signals $\Lambda_c^{*+} \to \Lambda_c^+\pi^0\pi^0$, they also contribute events to the resonances $\Lambda_c(2595)^+$ and $\Lambda_c(2625)^+$. These backgrounds will be subtracted from the signal yields in the fit_{sig}, denoted as the term "$N^{\text{obs}}_{\Lambda_c^{*+}} - N_{\text{bkg}}$" in Equation 3.1. The $\Lambda_c^{*+} \to \Lambda_c^+\pi^+\pi^-$ backgrounds are estimated using the corresponding exclusive MC samples, and their event yields are normalised with $\mathcal{B}(\Lambda_c(2595)^+ \to \Lambda_c^+\pi^+\pi^-) = (66.0 \pm 14.1_{\text{stat.}})\%$ [7] and $\mathcal{B}(\Lambda_c(2625)^+ \to \Lambda_c^+\pi^+\pi^-) = (51.1 \pm 5.8_{\text{stat.}} \pm 3.5_{\text{syst.}})\%$ [9], respectively. This results into 7.5 and 5.7 events for $\Lambda_c(2595)^+ \to \Lambda_c^+\pi^+\pi^-$ background, and 5.5 and 3.4 events for $\Lambda_c(2625)^+ \to \Lambda_c^+\pi^+\pi^-$ background at $\sqrt{s} = 4.918\,\text{GeV}$ and $\sqrt{s} = 4.951\,\text{GeV}$, respectively. Another potential source of peaking backgrounds is the processes $\Lambda_c^{*+} \to \Lambda_c^+\gamma$. However, the decay $\Lambda_c^{*+} \to \Lambda_c^+\gamma$ has not been observed [7]. Therefore, the contributions are estimated by conservatively assigning $\mathcal{B}(\Lambda_c(2595)^+ \to \Lambda_c^+\gamma) = 5.0\%$ and $\mathcal{B}(\Lambda_c(2625)^+ \to \Lambda_c^+\gamma) = 5.0\%$. This results into 1.7 and 1.3 events for $\Lambda_c(2595)^+ \to \Lambda_c^+\gamma$, and 1.3 and 0.8 for $\Lambda_c(2625)^+ \to \Lambda_c^+\gamma$ at $\sqrt{s} = 4.918$ and 4.951 GeV, respectively. The contamination from $\Lambda_c^{*+} \to \Lambda_c^+\gamma$ backgrounds is considered negligible. The obtained signal yields are listed in table 1.

Due to inconsistencies in the information of fake photons between data and MC simulation, the efficiency of the requirement on N_{π^0}, obtained from signal MC samples, needs to be corrected. A control sample of $e^+e^- \to \Lambda_c^+\bar{\Lambda}_c^-$ with $\bar{\Lambda}_c^-$ decaying into the three tag modes and Λ_c^+ to any allowed processes is selected using the data set at $\sqrt{s} = 4.68\,\text{GeV}$. This control sample exhibits a photon environment comparable to that of the signal $e^+e^- \to \bar{\Lambda}_c^-\Lambda_c^{*+}$ with $\Lambda_c^{*+} \to \Lambda_c^+\pi^0\pi^0$ and $\bar{\Lambda}_c^-$ decaying into the three tag modes, excluding the γ's from the signal π^0's. To replicate the photon environment in data for the signal processes, a mixed sample is created. Each event in the mixed sample comprises non-signal γ's from the control sample and signal γ's from the decay of the π^0's, which are the daughter particles of Λ_c^{*+}. The signal γ's are obtained from the signal MC samples. All the non-signal and signal γ's are randomly selected from the control sample and signal MC samples at the reconstruction level, respectively, and they are combined to form an event in the mixed sample. The π^0 candidates are then reconstructed with any photon pairs in each event of the mixed sample. Subsequently, the requirement on N_{π^0} is applied to both the signal MC samples and the mixed sample, and the corresponding selection efficiencies are determined to be 0.2327 and 0.2132, respectively. Their ratio, 0.92, is assigned as the correction factor in the efficiencies ϵ_{sig}.

The BFs of $\Lambda_c(2595)^+ \to \Lambda_c^+\pi^0\pi^0$ and $\Lambda_c(2625)^+ \to \Lambda_c^+\pi^0\pi^0$ are determined to be $(59.5 \pm 11.1_{\text{stat.}})\%$ and $(41.0 \pm 5.2_{\text{stat.}})\%$, respectively, where the uncertainties are statistical. Two toy MC samples are generated using the Probability Density Function (PDF) of $\mathcal{B}(\Lambda_c(2625)^+ \to \Lambda_c^+\pi^0\pi^0)$ and $\mathcal{B}(\Lambda_c(2625)^+ \to \Lambda_c^+\pi^+\pi^-)$ after cancelling the uncertainties from tag yields, and a set of the corresponding ratio of these two BFs is obtained. The ratio of the BFs between $\Lambda_c(2625)^+ \to \Lambda_c^+\pi^0\pi^0$ and $\Lambda_c(2625)^+ \to \Lambda_c^+\pi^+\pi^-$ is determined to be 0.8 ± 0.2.

JHEP08(2025)065

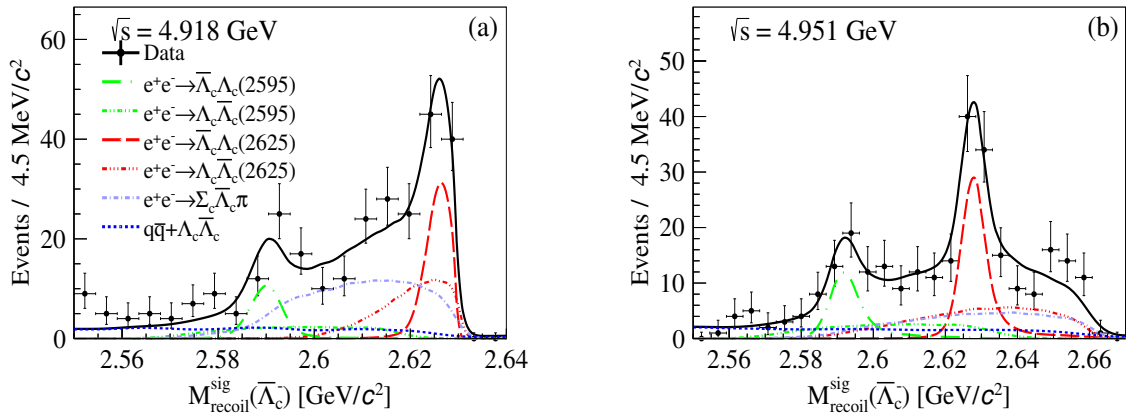

Figure 2. The fits to the distributions $M^{\rm sig}_{\rm recoil}(\bar{\Lambda}_c^-)$ at $\sqrt{s} = 4.918\,\text{GeV}$ (a) and 4.951 GeV (b). The black points with error bars are data. The solid curves represent the fit results, and the dashed curves describe individual components including both signals and backgrounds.

6 Systematic uncertainty

The systematic uncertainties in the BFs measurements primarily arise from the line shapes of cross sections, c.m. energy, beam energy spread, tag yield, efficiency correction of the N_{π^0} requirement, $\pi^\pm$ and γ vetoes, background estimation, and fit strategy. According to the Equation 3.1, the selection criteria of the tagged $\bar{\Lambda}_c^-$ affect both $\epsilon_{\rm tag}$ and $\epsilon_{\rm sig}$. Therefore, the systematic uncertainties in detection efficiency and $\mathcal{B}_{\rm tag}$ can be canceled out. All the systematic uncertainties are listed in table 3.

- **Line shapes of cross sections:** the uncertainties associated with the input line shapes of cross sections for $e^+e^- \to \Lambda_c^+\bar{\Lambda}_c(2595)^-$ and $e^+e^- \to \Lambda_c^+\bar{\Lambda}_c(2625)^-$ are studied by generating alternative MC samples with the cross sections varied by $\pm1\sigma$ [26] at $\sqrt{s} = 4.918$ and 4.951 GeV. The two maximum differences in BFs with respect to the nominal values are 2.8% and 2.1% for $\Lambda_c(2595)^+$ and $\Lambda_c(2625)^+$, respectively.

- **Centre-of-mass energy:** since $\sqrt{s} = 4.918\,\text{GeV}$ is close to the $\Lambda_c^+\bar{\Lambda}_c(2625)^-$ threshold, the $f_{\rm ISR}$ factor is highly sensitive to its actual energy value, where $f_{\rm ISR}$ is initial state radiation correction. In this analysis, the c.m. energy is measured to be $\sqrt{s} = 4918.02 \pm 0.34 \pm 0.34\,\text{MeV}$, and we obtain the systematic uncertainty in $f_{\rm ISR}$ at this point by varying the energy by $\pm1\sigma$. The maximum difference in resultant efficiencies between this case and the nominal one is regarded as the systematic uncertainty. The uncertainties are 0.4% and 3.3% for $\Lambda_c(2595)^+$ and $\Lambda_c(2625)^+$, respectively. For the other energy value, which is far from the threshold, the systematic uncertainties are negligible. The uncertainties at two energy values are weighted by the cross sections [26] and are assigned as 1.1% and 0.1% for $\Lambda_c(2595)^+$ and $\Lambda_c(2625)^+$, respectively.

- **Beam energy spread:** the beam energy spread has been estimated to be $1.55 \pm 0.18\,\text{MeV}$ at $\sqrt{s} = 4599.53\,\text{MeV}$ [28]. Then, it is calculated to be $1.77 \pm 0.20\,\text{MeV}$ at $\sqrt{s} = 4918.02\,\text{MeV}$ using the functions $\text{BES}_{4918.02} = \frac{4918.02^2}{4599.53^2}\cdot\text{BES}_{4599.53}$ and $\delta_{\text{BES}_{4918.02}} = \frac{\delta_{\text{BES}_{4599.53}}}{\text{BES}_{4599.53}} \cdot \frac{4918.02^2}{4599.53^2} \cdot \text{BES}_{4599.53}$ as described in ref. [29]. We obtain the systematic

JHEP08(2025)065

uncertainty at this energy point by generating alternative MC samples with the beam energy spread set to 1.57 MeV and 1.97 MeV. The difference in the resultant efficiencies is regarded as the systematic uncertainty. The uncertainties are 0.0% and 3.4% for $\Lambda_c(2595)^+$ and $\Lambda_c(2625)^+$, respectively. For the other energy point, the systematic uncertainties are negligible as it is far from the threshold. The uncertainties at the two energy points are weighted by the cross sections [26] and are assigned as 0.0% and 1.1% for $\Lambda_c(2595)^+$ and $\Lambda_c(2625)^+$, respectively.

- **Tag yields:** the uncertainty due to the tag yields cancels out. However, the uncertainty arising from background fluctuations in the tag yields contributes an additional uncertainty, which is determined to be $\sqrt{\sigma_{N_{\rm tag}} - N_{\rm tag}}$, where $\sigma_{N_{\rm tag}}$ is the statistical uncertainty obtained from the fit, and $N_{\rm tag}$ is the purely statistical uncertainty. The uncertainties are 10.4% and 5.2% for $\Lambda_c(2595)^+$ and $\Lambda_c(2625)^+$, respectively.

- **Efficiency correction of the N_{π^0} requirement:** the uncertainty in the efficiency correction of the N_{π^0} requirement arises from the statistical uncertainties in the yield of the mixed sample. The uncertainty, 1.2%, is assigned as the systematic uncertainty.

- **$\pi^\pm$ and γ vetoes:** we study the uncertainty of $\pi^\pm$ and γ vetoes together using a control sample of $\bar{\Lambda}_c^- \Lambda_c^+$ pair at $\sqrt{s} = 4.68\,\text{GeV}$, where $\bar{\Lambda}_c^- \to \bar{p}K^+\pi^-$ and Λ_c^+ decays to any allowed processes. After applying the $\pi^\pm$ and γ vetoes, the efficiency difference of between data and MC simulation is 0.7%, which is assigned as the systematic uncertainty.

- **Background estimation of $\Lambda_c^{*+} \to \Lambda_c^+\pi^+\pi^-$:** the uncertainty in background estimation of $\Lambda_c(2595)^+ \to \Lambda_c^+\pi^+\pi^-$ is evaluated by estimating the event yields of $\Lambda_c(2595)^+ \to \Lambda_c^+\pi^+\pi^-$ backgrounds using $\mathcal{B}(\Lambda_c(2595)^+ \to \Lambda_c^+\pi^+\pi^-) = (1 - 59.5\%)$. The new BF of $\Lambda_c(2595)^+ \to \Lambda_c^+\pi^0\pi^0$ is measured to be 63.9%. The difference of new BF and the nominal one is 7.4%. The uncertainty in background estimation of $\Lambda_c(2625)^+ \to \Lambda_c^+\pi^+\pi^-$ is estimated by quoting the BF uncertainty of $\Lambda_c(2625)^+ \to \Lambda_c^+\pi^+\pi^- = (50.7 \pm 5.0_{\rm stat.} \pm 4.9_{\rm syst.})\%$ from ref. [9]. The resultant uncertainties are 7.4% and 1.0% for $\Lambda_c(2595)^+$ and $\Lambda_c(2625)^+$, respectively.

- **Fit:** the uncertainty in the fitting strategy is also taken into account, which arises from:

  1. The uncertainty from the signal shape is estimated by changing the signal shape from the signal MC shape to the signal MC shape convolved with Gaussian functions with free parameters. The difference, 0.5%, is assigned as the uncertainty.
  2. The uncertainty arising from the estimation of the process $e^+e^- \to \Sigma_c\bar{\Lambda}_c^-\pi$: we obtain the systematic uncertainty in the line shape of the $\Sigma_c\bar{\Lambda}_c\pi$ by generating alternative MC samples with the input line shapes of cross sections changed to a flat line shape. The difference in resultant BFs is regarded as the systematic uncertainty. The uncertainties are 0.02% and 0.06% for $\Lambda_c(2595)^+$ and $\Lambda_c(2625)^+$, respectively, and we consider these uncertainties negligible. To estimate the uncertainty, we perform the fitting using only the shape of $e^+e^- \to \Sigma_c^+\bar{\Lambda}_c^-\pi^0$ instead of the original shape of $e^+e^- \to \Sigma_c\bar{\Lambda}_c^-\pi$, and we fix the yields of $e^+e^- \to \Sigma_c^+\bar{\Lambda}_c^-\pi^0$ based on the

JHEP08(2025)065

Source	$\Lambda_c(2595)^+ \to \Lambda_c^+\pi^0\pi^0$	$\Lambda_c(2625)^+ \to \Lambda_c^+\pi^0\pi^0$
Line shapes of cross sections	2.8	2.1
C.m. energy	1.1	0.1
Beam energy spread	0.0	1.1
Tag yield	10.4	5.2
Efficiency correction of the N_{π^0} requirement	1.2	1.2
$\pi^\pm$ and γ vetoes	0.7	0.7
Background estimation of $\Lambda_c^{*+} \to \Lambda_c^+\pi^+\pi^-$	7.4	1.0
Fit	1.9	5.6
Total	13.3	8.1

Table 3. Summary of systematic uncertainties (in %).

event number ratio of $e^+e^- \to \Sigma_c$ and Σ_c^+. The ratio is obtained from the study of $\Lambda_c^{*+} \to \Lambda_c^+\pi^+\pi^-$ [9]. The deviations of the fitted signal yields are treated as the systematic uncertainties, which are 1.9% and 5.6% for $\Lambda_c(2595)^+$ and $\Lambda_c(2625)^+$, respectively.

Table 3 summarises the sources of the systematic uncertainties in the BF measurements of $\Lambda_c(2595)^+$ and $\Lambda_c(2625)^+ \to \Lambda_c^+\pi^0\pi^0$. The total systematic uncertainties are calculated by adding all sources in quadrature, which are 13.3% and 8.1% for $\Lambda_c(2595)^+$ and $\Lambda_c(2625)^+$, respectively.

7 Summary

The strong decays $\Lambda_c(2595)^+ \to \Lambda_c^+\pi^0\pi^0$ and $\Lambda_c(2625)^+ \to \Lambda_c^+\pi^0\pi^0$ are measured using the 368.48 pb^{-1} of e^+e^- data collected at $\sqrt{s} = 4.918$ and 4.951 GeV with the BESIII detector at BEPCII. For the first time, the BF of $\Lambda_c(2595)^+ \to \Lambda_c^+\pi^0\pi^0$ is measured to be $(59.5 \pm 11.1_{\text{stat.}} \pm 7.9_{\text{syst.}})\%$, while the BF of $\Lambda_c(2625)^+ \to \Lambda_c^+\pi^0\pi^0$ is measured to be $(41.0 \pm 5.2_{\text{stat.}} \pm 3.3_{\text{syst.}})\%$. The absolute BF of the process $\Lambda_c(2625)^+ \to \Lambda_c^+\pi^+\pi^-$ at $\sqrt{s} = 4.918$ and 4.951 GeV has been measured to be $(51.1 \pm 5.8_{\text{stat.}} \pm 3.5_{\text{syst.}})\%$ [9]. The upper limit on the BF of decay $\Lambda_c(2595)^+ \to \Lambda_c^+\pi^+\pi^-$ is updated to be less than 58.0% at the 90% confidence level, based on the constraint $\mathcal{B}(\Lambda_c(2595)^+ \to \Lambda_c^+\pi^0\pi^0) + \mathcal{B}(\Lambda_c(2595)^+ \to \Lambda_c^+\pi^+\pi^-) <= 1$, where the uncertainty of $\mathcal{B}(\Lambda_c(2595)^+ \to \Lambda_c^+\pi^0\pi^0)$ has been taken into account. Table 4 shows a comparison of our BFs with the results of the $\Lambda_c^{*+} \to \Lambda_c^+\pi^+\pi^-$ decay. This analysis provides a model-independent measurement, representing the first experimental results for $\Lambda_c(2595)^+$ and $\Lambda_c(2625)^+ \to \Lambda_c^+\pi^0\pi^0$. This results will serve as an important inputs for calibrating relative measurements and guiding the search for unknown decays of $\Lambda_c(2595)^+$ and $\Lambda_c(2625)^+$. The ratio of $\mathcal{B}(\Lambda_c(2625)^+ \to \Lambda_c^+\pi^0\pi^0)$ to $\mathcal{B}(\Lambda_c(2625)^+ \to \Lambda_c^+\pi^+\pi^-)$ is calculated to be 0.8 ± 0.2 after cancelling the uncertainties from tag yields. The absolute BF of the process $\Lambda_c(2595)^+ \to \Lambda_c^+\pi^0\pi^0$ is consistent with the expected "threshold effect" within the uncertainty. However, further confirmation with additional data in the future is necessary.

JHEP08(2025)065

	PDG [7]	Measurements
$\mathcal{B}(\Lambda_c(2595)^+ \to \Lambda_c^+\pi^0\pi^0)$	–	$(59.5 \pm 11.1_{\text{stat.}} \pm 7.9_{\text{syst.}})\%$
$\mathcal{B}(\Lambda_c(2625)^+ \to \Lambda_c^+\pi^0\pi^0)$	–	$(41.0 \pm 5.2_{\text{stat.}} \pm 3.3_{\text{syst.}})\%$
$\mathcal{B}(\Lambda_c(2595)^+ \to \Lambda_c^+\pi^+\pi^-)$	–	$< 85.0\%$ [9]
$\mathcal{B}(\Lambda_c(2595)^+ \to \Lambda_c^+\pi^+\pi^-)$	–	$< 58.0\%$ estimated by this work
$\mathcal{B}(\Lambda_c(2625)^+ \to \Lambda_c^+\pi^+\pi^-)$	$\approx 67\%$	$(51.1 \pm 5.8_{\text{stat}} \pm 3.5_{\text{syst}})\%$ [9]

Table 4. Summary of the results.

Acknowledgments

The BESIII Collaboration thanks the staff of BEPCII and the IHEP computing center for their strong support. This work is supported in part by National Key R&D Program of China under Contracts Nos. 2023YFA1606000; National Natural Science Foundation of China (NSFC) under Contracts Nos. 11635010, 11735014, 11935015, 11935016, 11935018, 12025502, 12035009, 12035013, 12061131003, 12192260, 12192261, 12192262, 12192263, 12192264, 12192265, 12221005, 12225509, 12235017, 12361141819, 12475091; Guangzhou Navigation Project No. 2024A04J6334; the Chinese Academy of Sciences (CAS) Large-Scale Scientific Facility Program; the CAS Center for Excellence in Particle Physics (CCEPP); Joint Large-Scale Scientific Facility Funds of the NSFC and CAS under Contract No. U1832207; 100 Talents Program of CAS; The Institute of Nuclear and Particle Physics (INPAC) and Shanghai Key Laboratory for Particle Physics and Cosmology; German Research Foundation DFG under Contracts Nos. FOR5327, GRK 2149; Istituto Nazionale di Fisica Nucleare, Italy; Knut and Alice Wallenberg Foundation under Contracts Nos. 2021.0174, 2021.0299; Ministry of Development of Turkey under Contract No. DPT2006K-120470; National Research Foundation of Korea under Contract No. NRF-2022R1A2C1092335; National Science and Technology fund of Mongolia; National Science Research and Innovation Fund (NSRF) via the Program Management Unit for Human Resources & Institutional Development, Research and Innovation of Thailand under Contracts Nos. B16F640076, B50G670107; Polish National Science Centre under Contract No. 2019/35/O/ST2/02907; Swedish Research Council under Contract No. 2019.04595; The Swedish Foundation for International Cooperation in Research and Higher Education under Contract No. CH2018-7756; U.S. Department of Energy under Contract No. DE-FG02-05ER41374

Data Availability Statement. This article has no associated data or the data will not be deposited.

Code Availability Statement. This article has no associated code or the code will not be deposited.

JHEP08(2025)065

References

[1] H.-Y. Cheng and C.-K. Chua, *Strong Decays of Charmed Baryons in Heavy Hadron Chiral Perturbation Theory*, *Phys. Rev. D* **75** (2007) 014006 [hep-ph/0610283] [INSPIRE].

[2] H.-Y. Cheng and C.-K. Chua, *Strong Decays of Charmed Baryons in Heavy Hadron Chiral Perturbation Theory: An Update*, *Phys. Rev. D* **92** (2015) 074014 [arXiv:1508.05653] [INSPIRE].

[3] T.-M. Yan et al., *Heavy quark symmetry and chiral dynamics*, *Phys. Rev. D* **46** (1992) 1148 [*Erratum ibid.* **55** (1997) 5851] [INSPIRE].

[4] D. Pirjol and T.-M. Yan, *Predictions for s wave and p wave heavy baryons from sum rules and constituent quark model. 1. Strong interactions*, *Phys. Rev. D* **56** (1997) 5483 [hep-ph/9701291] [INSPIRE].

[5] H.-Y. Cheng, *Charmed baryons circa 2015*, *Front. Phys. (Beijing)* **10** (2015) 101406 [INSPIRE].

[6] H.-Y. Cheng, *Charmed baryon physics circa 2021*, *Chin. J. Phys.* **78** (2022) 324 [arXiv:2109.01216] [INSPIRE].

[7] Particle Data Group collaboration, *Review of Particle Physics*, *PTEP* **2022** (2022) 083C01 [INSPIRE].

[8] Belle collaboration, *Measurement of the mass and width of the $\Lambda_c(2625)^+$ charmed baryon and the branching ratios of $\Lambda_c(2625)^+ \to \Sigma_c^0\pi^+$ and $\Lambda_c(2625)^+ \to \Sigma_c^+ + \pi^-$*, *Phys. Rev. D* **107** (2023) 032008 [arXiv:2212.04062] [INSPIRE].

[9] BESIII collaboration, *First measurements of the absolute branching fraction of $\Lambda_c(2625)^+ \to \Lambda_c + \pi^+\pi^-$ and upper limit on $\Lambda_c(2595)^+ \to \Lambda_c + \pi^+\pi^-$*, *Phys. Rev. D* **109** (2024) 112007 [arXiv:2401.09225] [INSPIRE].

[10] A.E. Blechman, A.F. Falk, D. Pirjol and J.M. Yelton, *Threshold effects in excited charmed baryon decays*, *Phys. Rev. D* **67** (2003) 074033 [hep-ph/0302040] [INSPIRE].

[11] B.-C. Ke, J. Koponen, H.-B. Li and Y. Zheng, *Recent Progress in Leptonic and Semileptonic Decays of Charmed Hadrons*, *Ann. Rev. Nucl. Part. Sci.* **73** (2023) 285 [arXiv:2310.05228] [INSPIRE].

[12] BESIII collaboration, *Luminosities and energies of e^+e^- collision data taken between =4.61 GeV and 4.95 GeV at BESIII*, *Chin. Phys. C* **46** (2022) 113003 [arXiv:2205.04809] [INSPIRE].

[13] BESIII collaboration, *Design and Construction of the BESIII Detector*, *Nucl. Instrum. Meth. A* **614** (2010) 345 [arXiv:0911.4960] [INSPIRE].

[14] C. Yu et al., *BEPCII Performance and Beam Dynamics Studies on Luminosity*, in the proceedings of the *7th International Particle Accelerator Conference*, Busan, South Korea, May 08–13 (2016) [DOI:10.18429/JACoW-IPAC2016-TUYA01] [INSPIRE].

[15] BESIII collaboration, *Future Physics Programme of BESIII*, *Chin. Phys. C* **44** (2020) 040001 [arXiv:1912.05983] [INSPIRE].

[16] K.-X. Huang et al., *Method for detector description transformation to Unity and application in BESIII*, *Nucl. Sci. Tech.* **33** (2022) 142 [arXiv:2206.10117] [INSPIRE].

[17] X. Li et al., *Study of MRPC technology for BESIII endcap-TOF upgrade*, *Radiat. Detect. Technol. Methods* **1** (2017) 13 [INSPIRE].

[18] Y.-X. Guo et al., *The study of time calibration for upgraded end cap TOF of BESIII*, *Radiat. Detect. Technol. Methods* **1** (2017) 15 [INSPIRE].

JHEP08(2025)065

[19] GEANT4 collaboration, *GEANT4 - A Simulation Toolkit*, *Nucl. Instrum. Meth. A* **506** (2003) 250 [INSPIRE].

[20] D.J. Lange, *The EvtGen particle decay simulation package*, *Nucl. Instrum. Meth. A* **462** (2001) 152 [INSPIRE].

[21] R.-G. Ping, *Event generators at BESIII*, *Chin. Phys. C* **32** (2008) 599 [INSPIRE].

[22] J.C. Chen et al., *Event generator for J/ψ and $\psi(2S)$ decay*, *Phys. Rev. D* **62** (2000) 034003 [INSPIRE].

[23] R.-L. Yang, R.-G. Ping and H. Chen, *Tuning and Validation of the Lundcharm Model with J/ψ Decays*, *Chin. Phys. Lett.* **31** (2014) 061301 [INSPIRE].

[24] E. Richter-Was, *QED bremsstrahlung in semileptonic B and leptonic tau decays*, *Phys. Lett. B* **303** (1993) 163 [INSPIRE].

[25] S. Jadach, B.F.L. Ward and Z. Was, *Coherent exclusive exponentiation for precision Monte Carlo calculations*, *Phys. Rev. D* **63** (2001) 113009 [hep-ph/0006359] [INSPIRE].

[26] BESIII collaboration, *Measurements of Born cross sections for $e^+e^- \to \Lambda_c^+\bar{\Lambda}_c(2595)^- + c.c.$ and $e^+e^- \to \Lambda_c^+\bar{\Lambda}_c(2625)^- + c.c.$ at $\sqrt{s} = 4918.0$ and 4950.9 MeV*, *Phys. Rev. D* **109** (2024) L071104 [arXiv:2312.08414] [INSPIRE].

[27] ARGUS collaboration, *Search for Hadronic $b \to u$ Decays*, *Phys. Lett. B* **241** (1990) 278 [INSPIRE].

[28] BESIII collaboration, *Precision measurement of the $e^+e^- \to \Lambda_c^+\bar{\Lambda}_c^-$ cross section near threshold*, *Phys. Rev. Lett.* **120** (2018) 132001 [arXiv:1710.00150] [INSPIRE].

[29] M. Sands et al., *The physics of electron storage rings. An introduction*, SLAC-r-121, (1970).

JHEP08(2025)065

The BESIII collaboration

M. Ablikim[1], M.N. Achasov[4,c], P. Adlarson[76], O. Afedulidis[3], X.C. Ai[81], R. Aliberti[35], A. Amoroso[75A,75C], Y. Bai[57], O. Bakina[36], I. Balossino[29A], Y. Ban[46,h], H.-R. Bao[64], V. Batozskaya[1,44], K. Begzsuren[32], N. Berger[35], M. Berlowski[44], M. Bertani[28A], D. Bettoni[29A], F. Bianchi[75A,75C], E. Bianco[75A,75C], A. Bortone[75A,75C], I. Boyko[36], R.A. Briere[5], A. Brueggemann[69], H. Cai[77], X. Cai[1,58], A. Calcaterra[28A], G.F. Cao[1,64], N. Cao[1,64], S.A. Cetin[62A], X.Y. Chai[46,h], J.F. Chang[1,58], G.R. Che[43], Y.Z. Che[1,58,64], G. Chelkov[36,b], C. Chen[43], C.H. Chen[9], Chao Chen[55], G. Chen[1], H.S. Chen[1,64], H.Y. Chen[20], M.L. Chen[1,58,64], S.J. Chen[42], S.L. Chen[45], S.M. Chen[61], T. Chen[1,64], X.R. Chen[31,64], X.T. Chen[1,64], Y.B. Chen[1,58], Y.Q. Chen[34], Z.J. Chen[25,i], S.K. Choi[10], G. Cibinetto[29A], F. Cossio[75C], J.J. Cui[50], H.L. Dai[1,58], J.P. Dai[79], A. Dbeyssi[18], R. E. de Boer[3], D. Dedovich[36], C.Q. Deng[73], Z.Y. Deng[1], A. Denig[35], I. Denysenko[36], M. Destefanis[75A,75C], F. De Mori[75A,75C], B. Ding[67,1], X.X. Ding[46,h], Y. Ding[40], Y. Ding[34], J. Dong[1,58], L.Y. Dong[1,64], M.Y. Dong[1,58,64], X. Dong[77], M.C. Du[1], S.X. Du[81], Y.Y. Duan[55], Z.H. Duan[42], P. Egorov[36,b], G.F. Fan[42], J.J. Fan[19], Y.H. Fan[45], J. Fang[1,58], J. Fang[59], S.S. Fang[1,64], W.X. Fang[1], Y. Fang[1], Y.Q. Fang[1,58], R. Farinelli[29A], L. Fava[75B,75C], F. Feldbauer[3], G. Felici[28A], C.Q. Feng[72,58], J.H. Feng[59], Y.T. Feng[72,58], M. Fritsch[3], C.D. Fu[1], J.L. Fu[64], Y.W. Fu[1,64], H. Gao[64], X.B. Gao[41], Y.N. Gao[46,h], Y.N. Gao[19], Yang Gao[72,58], S. Garbolino[75C], I. Garzia[29A,29B], P.T. Ge[19], Z.W. Ge[42], C. Geng[59], E.M. Gersabeck[68], A. Gilman[70], K. Goetzen[13], L. Gong[40], W.X. Gong[1,58], W. Gradl[35], S. Gramigna[29A,29B], M. Greco[75A,75C], M.H. Gu[1,58], Y.T. Gu[15], C.Y. Guan[1,64], A.Q. Guo[31,64], L.B. Guo[41], M.J. Guo[50], R.P. Guo[49], Y.P. Guo[12,g], A. Guskov[36,b], J. Gutierrez[27], K.L. Han[64], T.T. Han[1], F. Hanisch[3], X.Q. Hao[19], F.A. Harris[66], K.K. He[55], K.L. He[1,64], F.H. Heinsius[3], C.H. Heinz[35], Y.K. Heng[1,58,64], C. Herold[60], T. Holtmann[3], P.C. Hong[34], G.Y. Hou[1,64], X.T. Hou[1,64], Y.R. Hou[64], Z.L. Hou[1], B.Y. Hu[59], H.M. Hu[1,64], J.F. Hu[56,j], Q.P. Hu[72,58], S.L. Hu[12,g], T. Hu[1,58,64], Y. Hu[1], G.S. Huang[72,58], K.X. Huang[59], L.Q. Huang[31,64], P. Huang[42], X.T. Huang[50], Y.P. Huang[1], Y.S. Huang[59], T. Hussain[74], F. Hölzken[3], N. Hüsken[35], N. in der Wiesche[69], J. Jackson[27], S. Janchiv[32], Q. Ji[1], Q.P. Ji[19], W. Ji[1,64], X.B. Ji[1,64], X.L. Ji[1,58], Y.Y. Ji[50], X.Q. Jia[50], Z.K. Jia[72,58], D. Jiang[1,64], H.B. Jiang[77], P.C. Jiang[46,h], S.S. Jiang[39], T.J. Jiang[16], X.S. Jiang[1,58,64], Y. Jiang[64], J.B. Jiao[50], J.K. Jiao[34], Z. Jiao[23], S. Jin[42], Y. Jin[67], M.Q. Jing[1,64], X.M. Jing[64], T. Johansson[76], S. Kabana[33], N. Kalantar-Nayestanaki[65], X.L. Kang[9], X.S. Kang[40], M. Kavatsyuk[65], B.C. Ke[81], V. Khachatryan[27], A. Khoukaz[69], R. Kiuchi[1], O.B. Kolcu[62A], B. Kopf[3], M. Kuessner[3], X. Kui[1,64], N. Kumar[26], A. Kupsc[44,76], W. Kühn[37], W.N. Lan[19], T.T. Lei[72,58], Z.H. Lei[72,58], M. Lellmann[35], T. Lenz[35], C. Li[43], C. Li[47], C.H. Li[39], Cheng Li[72,58], D.M. Li[81], F. Li[1,58], G. Li[1], H.B. Li[1,64], H.J. Li[19], H.N. Li[56,j], Hui Li[43], J.R. Li[61], J.S. Li[59], K. Li[1], K.L. Li[19], L.J. Li[1,64], L.K. Li[1], Lei Li[48], M.H. Li[43], P.L. Li[64], P.R. Li[38,k,l], Q.M. Li[1,64], Q.X. Li[50], R. Li[17,31], T. Li[50], T.Y. Li[43], W.D. Li[1,64], W.G. Li[1,a], X. Li[1,64], X.H. Li[72,58], X.L. Li[50], X.Y. Li[1,8], X.Z. Li[59], Y. Li[19], Y.G. Li[46,h], Z.J. Li[59], Z.Y. Li[79], C. Liang[42], H. Liang[72,58], H. Liang[1,64], Y.F. Liang[54], Y.T. Liang[31,64], G.R. Liao[14], Y.P. Liao[1,64], J. Libby[26], A. Limphirat[60], C.C. Lin[55], C.X. Lin[64], D.X. Lin[31,64], T. Lin[1], B.J. Liu[1], B.X. Liu[77], C. Liu[34], C.X. Liu[1], F. Liu[1], F.H. Liu[53], Feng Liu[6], G.M. Liu[56,j], H. Liu[38,k,l], H.B. Liu[15], H.H. Liu[1], H.M. Liu[1,64], Huihui Liu[21], J.B. Liu[72,58], J.Y. Liu[1,64], K. Liu[38,k,l], K.Y. Liu[40], Ke Liu[22], L. Liu[72,58], L.C. Liu[43], Lu Liu[43], M.H. Liu[12,g], P.L. Liu[1], Q. Liu[64], S.B. Liu[72,58], T. Liu[12,g], W.K. Liu[43], W.M. Liu[72,58], X. Liu[38,k,l], X. Liu[39], Y. Liu[38,k,l], Y. Liu[81], Y.B. Liu[43], Z.A. Liu[1,58,64], Z.D. Liu[9], Z.Q. Liu[50], X.C. Lou[1,58,64], F.X. Lu[59], H.J. Lu[23], J.G. Lu[1,58], Y. Lu[7], Y.P. Lu[1,58], Z.H. Lu[1,64], C.L. Luo[41], J.R. Luo[59], M.X. Luo[80], T. Luo[12,g], X.L. Luo[1,58], X.R. Lyu[64], Y.F. Lyu[43],

JHEP08(2025)065

F.C. Ma[40], H. Ma[79], H.L. Ma[1], J.L. Ma[1,64], L.L. Ma[50], L.R. Ma[67], M.M. Ma[1,64], Q.M. Ma[1], R.Q. Ma[1,64], R.Y. Ma[19], T. Ma[72,58], X.T. Ma[1,64], X.Y. Ma[1,58], Y.M. Ma[31], F.E. Maas[18], I. MacKay[70], M. Maggiora[75A,75C], S. Malde[70], Y.J. Mao[46,h], Z.P. Mao[1], S. Marcello[75A,75C], Y.H. Meng[64], Z.X. Meng[67], J.G. Messchendorp[13,65], G. Mezzadri[29A], H. Miao[1,64], T.J. Min[42], R.E. Mitchell[27], X.H. Mo[1,58,64], B. Moses[27], N. Yu. Muchnoi[4,c], J. Muskalla[35], Y. Nefedov[36], F. Nerling[18,e], L.S. Nie[20], I.B. Nikolaev[4,c], Z. Ning[1,58], S. Nisar[11,m], Q.L. Niu[38,k,l], W.D. Niu[55], Y. Niu [50], S.L. Olsen[10,64], Q. Ouyang[1,58,64], S. Pacetti[28B,28C], X. Pan[55], Y. Pan[57], A. Pathak[10], Y.P. Pei[72,58], M. Pelizaeus[3], H.P. Peng[72,58], Y.Y. Peng[38,k,l], K. Peters[13,e], J.L. Ping[41], R.G. Ping[1,64], S. Plura[35], V. Prasad[33], F.Z. Qi[1], H. Qi[72,58], H.R. Qi[61], M. Qi[42], S. Qian[1,58], W.B. Qian[64], C.F. Qiao[64], J.H. Qiao[19], J.J. Qin[73], L.Q. Qin[14], L.Y. Qin[72,58], X.P. Qin[12,g], X.S. Qin[50], Z.H. Qin[1,58], J.F. Qiu[1], Z.H. Qu[73], C.F. Redmer[35], K.J. Ren[39], A. Rivetti[75C], M. Rolo[75C], G. Rong[1,64], Ch. Rosner[18], M.Q. Ruan[1,58], S.N. Ruan[43], N. Salone[44], A. Sarantsev[36,d], Y. Schelhaas[35], K. Schoenning[76], M. Scodeggio[29A], K.Y. Shan[12,g], W. Shan[24], X.Y. Shan[72,58], Z.J. Shang[38,k,l], J.F. Shangguan[16], L.G. Shao[1,64], M. Shao[72,58], C.P. Shen[12,g], H.F. Shen[1,8], W.H. Shen[64], X.Y. Shen[1,64], B.A. Shi[64], H. Shi[72,58], J.L. Shi[12,g], J.Y. Shi[1], S.Y. Shi[73], X. Shi[1,58], J.J. Song[19], T.Z. Song[59], W.M. Song[34,1], Y. J. Song[12,g], Y.X. Song[46,h,n], S. Sosio[75A,75C], S. Spataro[75A,75C], F. Stieler[35], S. S Su[40], Y.J. Su[64], G.B. Sun[77], G.X. Sun[1], H. Sun[64], H.K. Sun[1], J.F. Sun[19], K. Sun[61], L. Sun[77], S.S. Sun[1,64], T. Sun[51,f], Y.J. Sun[72,58], Y.Z. Sun[1], Z.Q. Sun[1,64], Z.T. Sun[50], C.J. Tang[54], G.Y. Tang[1], J. Tang[59], M. Tang[72,58], Y.A. Tang[77], L.Y. Tao[73], Q.T. Tao[25,i], M. Tat[70], J.X. Teng[72,58], V. Thoren[76], W.H. Tian[59], Y. Tian[31,64], Z.F. Tian[77], I. Uman[62B], Y. Wan[55], S.J. Wang[50], B. Wang[1], Bo Wang[72,58], C. Wang[19], D.Y. Wang[46,h], H.J. Wang[38,k,l], J.J. Wang[77], J.P. Wang [50], K. Wang[1,58], L.L. Wang[1], L.W. Wang[34], M. Wang[50], N.Y. Wang[64], S. Wang[38,k,l], S. Wang[12,g], T. Wang[12,g], T.J. Wang[43], W. Wang[59], W. Wang[73], W.P. Wang[35,58,72,o], X. Wang[46,h], X.F. Wang[38,k,l], X.J. Wang[39], X.L. Wang[12,g], X.N. Wang[1], Y. Wang[61], Y.D. Wang[45], Y.F. Wang[1,58,64], Y.H. Wang[38,k,l], Y.L. Wang[19], Y.N. Wang[45], Y.Q. Wang[1], Yaqian Wang[17], Yi Wang[61], Z. Wang[1,58], Z.L. Wang[73], Z.Y. Wang[1,64], D.H. Wei[14], F. Weidner[69], S.P. Wen[1], Y.R. Wen[39], U. Wiedner[3], G. Wilkinson[70], M. Wolke[76], L. Wollenberg[3], C. Wu[39], J.F. Wu[1,8], L.H. Wu[1], L.J. Wu[1,64], Lianjie Wu[19], X. Wu[12,g], X.H. Wu[34], Y.H. Wu[55], Y.J. Wu[31], Z. Wu[1,58], L. Xia[72,58], X.M. Xian[39], B.H. Xiang[1,64], T. Xiang[46,h], D. Xiao[38,k,l], G.Y. Xiao[42], H. Xiao[73], S.Y. Xiao[1], Y. L. Xiao[12,g], Z.J. Xiao[41], C. Xie[42], X.H. Xie[46,h], Y. Xie[50], Y.G. Xie[1,58], Y.H. Xie[6], Z.P. Xie[72,58], T.Y. Xing[1,64], C.F. Xu[1,64], C.J. Xu[59], G.F. Xu[1], M. Xu[72,58], Q.J. Xu[16], Q.N. Xu[30], W.L. Xu[67], X.P. Xu[55], Y. Xu[40], Y.C. Xu[78], Z.S. Xu[64], F. Yan[12,g], L. Yan[12,g], W.B. Yan[72,58], W.C. Yan[81], W.P. Yan[19], X.Q. Yan[1,64], H.J. Yang[51,f], H.L. Yang[34], H.X. Yang[1], J.H. Yang[42], R.J. Yang[19], T. Yang[1], Y. Yang[12,g], Y.F. Yang[1,64], Y.F. Yang[43], Y.X. Yang[1,64], Y.Z. Yang[19], Z.W. Yang[38,k,l], Z.P. Yao[50], M. Ye[1,58], M.H. Ye[8], J.H. Yin[1], Junhao Yin[43], Z.Y. You[59], B.X. Yu[1,58,64], C.X. Yu[43], G. Yu[1,64], J.S. Yu[25,i], M.C. Yu[40], T. Yu[73], X.D. Yu[46,h], C.Z. Yuan[1,64], J. Yuan[45], J. Yuan[34], L. Yuan[2], S.C. Yuan[1,64], Y. Yuan[1,64], Z.Y. Yuan[59], C.X. Yue[39], Ying Yue[19], A.A. Zafar[74], F.R. Zeng[50], S.H. Zeng[63], X. Zeng[12,g], Y. Zeng[25,i], Y.J. Zeng[59], Y.J. Zeng[1,64], X.Y. Zhai[34], Y.C. Zhai[50], Y.H. Zhan[59], A.Q. Zhang[1,64], B.L. Zhang[1,64], B.X. Zhang[1], D.H. Zhang[43], G.Y. Zhang[19], H. Zhang[72,58], H. Zhang[81], H.C. Zhang[1,58,64], H.H. Zhang[59], H.Q. Zhang[1,58,64], H.R. Zhang[72,58], H.Y. Zhang[1,58], J. Zhang[81], J. Zhang[59], J.J. Zhang[52], J.L. Zhang[20], J.Q. Zhang[41], J.S. Zhang[12,g], J.W. Zhang[1,58,64], J.X. Zhang[38,k,l], J.Y. Zhang[1], J.Z. Zhang[1,64], Jianyu Zhang[64], L.M. Zhang[61], Lei Zhang[42], P. Zhang[1,64], Q. Zhang[19], Q.Y. Zhang[34], R.Y. Zhang[38,k,l], S.H. Zhang[1,64], Shulei Zhang[25,i],

JHEP08(2025)065

X.M. Zhang[1], X. Y Zhang[40], X.Y. Zhang[50], Y. Zhang[73], Y. Zhang[1], Y. T. Zhang[81], Y.H. Zhang[1,58], Y.M. Zhang[39], Yan Zhang[72,58], Z.D. Zhang[1], Z.H. Zhang[1], Z.L. Zhang[34], Z.X. Zhang[19], Z.Y. Zhang[43], Z.Y. Zhang[77], Z.Z. Zhang[45], Zh. Zh. Zhang[19], G. Zhao[1], J.Y. Zhao[1,64], J.Z. Zhao[1,58], L. Zhao[1], Lei Zhao[72,58], M.G. Zhao[43], N. Zhao[79], R.P. Zhao[64], S.J. Zhao[81], Y.B. Zhao[1,58], Y.X. Zhao[31,64], Z.G. Zhao[72,58], A. Zhemchugov[36,b], B. Zheng[73], B.M. Zheng[34], J.P. Zheng[1,58], W.J. Zheng[1,64], X.R. Zheng[19], Y.H. Zheng[64], B. Zhong[41], X. Zhong[59], H. Zhou[35,50,o], J.Y. Zhou[34], L.P. Zhou[1,64], S. Zhou[6], X. Zhou[77], X.K. Zhou[6], X.R. Zhou[72,58], X.Y. Zhou[39], Y.Z. Zhou[12,g], Z.C. Zhou[20], A.N. Zhu[64], J. Zhu[43], K. Zhu[1], K.J. Zhu[1,58,64], K.S. Zhu[12,g], L. Zhu[34], L.X. Zhu[64], S.H. Zhu[71], T.J. Zhu[12,g], W.D. Zhu[41], W.Z. Zhu[19], Y.C. Zhu[72,58], Z.A. Zhu[1,64], J.H. Zou[1], J. Zu[72,58]

[1] *Institute of High Energy Physics, Beijing 100049, People's Republic of China*
[2] *Beihang University, Beijing 100191, People's Republic of China*
[3] *Bochum Ruhr-University, D-44780 Bochum, Germany*
[4] *Budker Institute of Nuclear Physics SB RAS (BINP), Novosibirsk 630090, Russia*
[5] *Carnegie Mellon University, Pittsburgh, Pennsylvania 15213, U.S.A.*
[6] *Central China Normal University, Wuhan 430079, People's Republic of China*
[7] *Central South University, Changsha 410083, People's Republic of China*
[8] *China Center of Advanced Science and Technology, Beijing 100190, People's Republic of China*
[9] *China University of Geosciences, Wuhan 430074, People's Republic of China*
[10] *Chung-Ang University, Seoul, 06974, Republic of Korea*
[11] *COMSATS University Islamabad, Lahore Campus, Defence Road, Off Raiwind Road, 54000 Lahore, Pakistan*
[12] *Fudan University, Shanghai 200433, People's Republic of China*
[13] *GSI Helmholtzcentre for Heavy Ion Research GmbH, D-64291 Darmstadt, Germany*
[14] *Guangxi Normal University, Guilin 541004, People's Republic of China*
[15] *Guangxi University, Nanning 530004, People's Republic of China*
[16] *Hangzhou Normal University, Hangzhou 310036, People's Republic of China*
[17] *Hebei University, Baoding 071002, People's Republic of China*
[18] *Helmholtz Institute Mainz, Staudinger Weg 18, D-55099 Mainz, Germany*
[19] *Henan Normal University, Xinxiang 453007, People's Republic of China*
[20] *Henan University, Kaifeng 475004, People's Republic of China*
[21] *Henan University of Science and Technology, Luoyang 471003, People's Republic of China*
[22] *Henan University of Technology, Zhengzhou 450001, People's Republic of China*
[23] *Huangshan College, Huangshan 245000, People's Republic of China*
[24] *Hunan Normal University, Changsha 410081, People's Republic of China*
[25] *Hunan University, Changsha 410082, People's Republic of China*
[26] *Indian Institute of Technology Madras, Chennai 600036, India*
[27] *Indiana University, Bloomington, Indiana 47405, U.S.A.*
[28] *INFN Laboratori Nazionali di Frascati , (A)INFN Laboratori Nazionali di Frascati, I-00044, Frascati, Italy; (B)INFN Sezione di Perugia, I-06100, Perugia, Italy; (C)University of Perugia, I-06100, Perugia, Italy*
[29] *INFN Sezione di Ferrara, (A)INFN Sezione di Ferrara, I-44122, Ferrara, Italy; (B)University of Ferrara, I-44122, Ferrara, Italy*
[30] *Inner Mongolia University, Hohhot 010021, People's Republic of China*
[31] *Institute of Modern Physics, Lanzhou 730000, People's Republic of China*
[32] *Institute of Physics and Technology, Peace Avenue 54B, Ulaanbaatar 13330, Mongolia*
[33] *Instituto de Alta Investigación, Universidad de Tarapacá, Casilla 7D, Arica 1000000, Chile*
[34] *Jilin University, Changchun 130012, People's Republic of China*
[35] *Johannes Gutenberg University of Mainz, Johann-Joachim-Becher-Weg 45, D-55099 Mainz, Germany*
[36] *Joint Institute for Nuclear Research, 141980 Dubna, Moscow region, Russia*
[37] *Justus-Liebig-Universitaet Giessen, II. Physikalisches Institut, Heinrich-Buff-Ring 16, D-35392 Giessen, Germany*

JHEP08(2025)065

[38] Lanzhou University, Lanzhou 730000, People's Republic of China
[39] Liaoning Normal University, Dalian 116029, People's Republic of China
[40] Liaoning University, Shenyang 110036, People's Republic of China
[41] Nanjing Normal University, Nanjing 210023, People's Republic of China
[42] Nanjing University, Nanjing 210093, People's Republic of China
[43] Nankai University, Tianjin 300071, People's Republic of China
[44] National Centre for Nuclear Research, Warsaw 02-093, Poland
[45] North China Electric Power University, Beijing 102206, People's Republic of China
[46] Peking University, Beijing 100871, People's Republic of China
[47] Qufu Normal University, Qufu 273165, People's Republic of China
[48] Renmin University of China, Beijing 100872, People's Republic of China
[49] Shandong Normal University, Jinan 250014, People's Republic of China
[50] Shandong University, Jinan 250100, People's Republic of China
[51] Shanghai Jiao Tong University, Shanghai 200240, People's Republic of China
[52] Shanxi Normal University, Linfen 041004, People's Republic of China
[53] Shanxi University, Taiyuan 030006, People's Republic of China
[54] Sichuan University, Chengdu 610064, People's Republic of China
[55] Soochow University, Suzhou 215006, People's Republic of China
[56] South China Normal University, Guangzhou 510006, People's Republic of China
[57] Southeast University, Nanjing 211100, People's Republic of China
[58] State Key Laboratory of Particle Detection and Electronics, Beijing 100049, Hefei 230026, People's Republic of China
[59] Sun Yat-Sen University, Guangzhou 510275, People's Republic of China
[60] Suranaree University of Technology, University Avenue 111, Nakhon Ratchasima 30000, Thailand
[61] Tsinghua University, Beijing 100084, People's Republic of China
[62] Turkish Accelerator Center Particle Factory Group, (A)Istinye University, 34010, Istanbul, Turkey; (B)Near East University, Nicosia, North Cyprus, 99138, Mersin 10, Turkey
[63] University of Bristol, H H Wills Physics Laboratory, Tyndall Avenue, Bristol, BS8 1TL, U.K.
[64] University of Chinese Academy of Sciences, Beijing 100049, People's Republic of China
[65] University of Groningen, NL-9747 AA Groningen, The Netherlands
[66] University of Hawaii, Honolulu, Hawaii 96822, U.S.A.
[67] University of Jinan, Jinan 250022, People's Republic of China
[68] University of Manchester, Oxford Road, Manchester, M13 9PL, United Kingdom
[69] University of Muenster, Wilhelm-Klemm-Strasse 9, 48149 Muenster, Germany
[70] University of Oxford, Keble Road, Oxford OX13RH, United Kingdom
[71] University of Science and Technology Liaoning, Anshan 114051, People's Republic of China
[72] University of Science and Technology of China, Hefei 230026, People's Republic of China
[73] University of South China, Hengyang 421001, People's Republic of China
[74] University of the Punjab, Lahore-54590, Pakistan
[75] University of Turin and INFN, (A)University of Turin, I-10125, Turin, Italy; (B)University of Eastern Piedmont, I-15121, Alessandria, Italy; (C)INFN, I-10125, Turin, Italy
[76] Uppsala University, Box 516, SE-75120 Uppsala, Sweden
[77] Wuhan University, Wuhan 430072, People's Republic of China
[78] Yantai University, Yantai 264005, People's Republic of China
[79] Yunnan University, Kunming 650500, People's Republic of China
[80] Zhejiang University, Hangzhou 310027, People's Republic of China
[81] Zhengzhou University, Zhengzhou 450001, People's Republic of China

[a] Deceased
[b] Also at the Moscow Institute of Physics and Technology, Moscow 141700, Russia
[c] Also at the Novosibirsk State University, Novosibirsk, 630090, Russia
[d] Also at the NRC "Kurchatov Institute", PNPI, 188300, Gatchina, Russia
[e] Also at Goethe University Frankfurt, 60323 Frankfurt am Main, Germany

JHEP08(2025)065

[f] Also at Key Laboratory for Particle Physics, Astrophysics and Cosmology, Ministry of Education; Shanghai Key Laboratory for Particle Physics and Cosmology; Institute of Nuclear and Particle Physics, Shanghai 200240, People's Republic of China
[g] Also at Key Laboratory of Nuclear Physics and Ion-beam Application (MOE) and Institute of Modern Physics, Fudan University, Shanghai 200443, People's Republic of China
[h] Also at State Key Laboratory of Nuclear Physics and Technology, Peking University, Beijing 100871, People's Republic of China
[i] Also at School of Physics and Electronics, Hunan University, Changsha 410082, China
[j] Also at Guangdong Provincial Key Laboratory of Nuclear Science, Institute of Quantum Matter, South China Normal University, Guangzhou 510006, China
[k] Also at MOE Frontiers Science Center for Rare Isotopes, Lanzhou University, Lanzhou 730000, People's Republic of China
[l] Also at Lanzhou Center for Theoretical Physics, Lanzhou University, Lanzhou 730000, People's Republic of China
[m] Also at the Department of Mathematical Sciences, IBA, Karachi 75270, Pakistan
[n] Also at Ecole Polytechnique Federale de Lausanne (EPFL), CH-1015 Lausanne, Switzerland
[o] Also at Helmholtz Institute Mainz, Staudinger Weg 18, D-55099 Mainz, Germany

JHEP08(2025)065